Complex electrophysiological remodeling in postinfarction ischemic heart failure

Bence Hegyi[a], Julie Bossuyt[a], Leigh G. Griffiths[b,c,d], Rafael Shimkunas[a,e], Zana Coulibaly[a], Zhong Jian[a], Kristin N. Grimsrud[f], Claus S. Sondergaard[f], Kenneth S. Ginsburg[a], Nipavan Chiamvimonvat[a,g,h], Luiz Belardinelli[i], András Varró[j,k], Julius G. Papp[j,k], Piero Pollesello[l], Jouko Levijoki[l], Leighton T. Izu[a], W. Douglas Boyd[f], Tamás Bányász[a,m], Donald M. Bers[a], and Ye Chen-Izu[a,e,g,1]

[a]Department of Pharmacology, University of California, Davis, CA 95616; [b]Department of Veterinary Medicine and Epidemiology, University of California, Davis, CA 95616; [c]Department of Cardiovascular Diseases, Mayo Clinic, Rochester, MN 55902; [d]College of Medicine, Mayo Clinic, Rochester, MN 55902; [e]Department of Biomedical Engineering, University of California, Davis, CA 95616; [f]Department of Surgery, University of California, Davis, Sacramento, CA 95817; [g]Division of Cardiovascular Medicine, Department of Internal Medicine, University of California, Davis, CA 95616; [h]Department of Veterans Affairs, Northern California Health Care System, Mather, CA 95655; [i]Department of Clinical Research, Gilead Sciences, Inc., Foster City, CA 94404; [j]Department of Pharmacology and Pharmacotherapy, Faculty of Medicine, University of Szeged, H-6720 Szeged, Hungary; [k]MTA-SZTE Research Group of Cardiovascular Pharmacology, Hungarian Academy of Sciences, H-6720 Szeged, Hungary; [l]Critical Care Proprietary Products, Orion Pharma, FI-02200 Espoo, Finland; and [m]Department of Physiology, Faculty of Medicine, University of Debrecen, H-4012 Debrecen, Hungary

Heart failure (HF) following myocardial infarction (MI) is associated with high incidence of cardiac arrhythmias. Development of therapeutic strategy requires detailed understanding of electrophysiological remodeling. However, changes of ionic currents in ischemic HF remain incompletely understood, especially in translational large-animal models. Here, we systematically measure the major ionic currents in ventricular myocytes from the infarct border and remote zones in a porcine model of post-MI HF. We recorded eight ionic currents during the cell's action potential (AP) under physiologically relevant conditions using [self]AP-clamp sequential dissection. Compared with healthy controls, HF-remote zone myocytes exhibited increased late Na$^+$ current, Ca^{2+}-activated K$^+$ current, Ca^{2+}-activated Cl$^-$ current, decreased rapid delayed rectifier K$^+$ current, and altered Na$^+$/Ca^{2+} exchange current profile. In HF-border zone myocytes, the above changes also occurred but with additional decrease of L-type Ca^{2+} current, decrease of inward rectifier K$^+$ current, and Ca^{2+} release-dependent delayed after-depolarizations. Our data reveal that the changes in any individual current are relatively small, but the integrated impacts shift the balance between the inward and outward currents to shorten AP in the border zone but prolong AP in the remote zone. This differential remodeling in post-MI HF increases the inhomogeneity of AP repolarization, which may enhance the arrhythmogenic substrate. Our comprehensive findings provide a mechanistic framework for understanding why single-channel blockers may fail to suppress arrhythmias, and highlight the need to consider the rich tableau and integration of many ionic currents in designing therapeutic strategies for treating arrhythmias in HF.

ischemic heart failure | myocardial infarction | electrophysiology | action potential | ionic currents

Ischemic cardiomyopathy as a chronic consequence of myocardial infarction (MI) represents a leading cause of heart failure (HF). Ischemic HF is characterized by extensive structural and functional remodeling that leads to altered action potential (AP) and increased susceptibility for cardiac arrhythmias (1). Precision therapeutic interventions require in-depth understanding of the electrophysiological changes that promote arrhythmias. However, the changes of ionic currents in ischemic HF remain incompletely understood to date, especially in large-animal models that are needed for translational studies. Emerging evidence suggests differential myocardium remodeling in the infarct border and remote zones, leading to complex changes in ionic currents (2), Ca^{2+} handling (3), and contractility (4). However, most previous studies were conducted either early after MI induction (in 2–7 d) or scar formation (within 8 wk) (2, 5), but not at the clinically relevant later stages of HF. Recently, we established a porcine MI model (6) that developed chronic HF (with reduced ejection fraction, EF)

over 5 mo, providing a large-animal model for translational study of chronic post-MI HF. In this study, we systematically investigated the changes of ionic currents and AP in ventricular myocytes from the infarct border and remote zones to gain a comprehensive understanding of the electrophysiological remodeling.

The AP of ventricular myocyte is shaped by a constellation of ionic currents that integrate at the cell level. The inward vs. outward currents counterbalance instantaneously to determine the AP profile. To gain a comprehensive view of remodeling, we developed an innovative [self]AP-clamp sequential dissection method (7) to record multiple inward and outward ionic currents during the cell's own AP under physiological conditions.

We found that HF remote-zone myocytes exhibit decreased rapid delayed rectifier K$^+$ current (I_{Kr}), altered Na$^+$/Ca^{2+} exchange current (I_{NCX}), and increases of late Na$^+$ current (I_{NaL}), Ca^{2+}-activated K$^+$ current [$I_{K(Ca)}$], and Ca^{2+}-activated Cl$^-$ current [$I_{Cl(Ca)}$]. The border-zone myocytes also show the above changes, but with

Significance

Cardiac arrhythmias often occur in heart failure (HF) patients, but drug therapies using selective ion channel blockers have failed clinical trials and effective drug therapies remain elusive. Here we systematically study the major ionic currents during the cardiac action potential (AP) and arrhythmogenic Ca^{2+} release in postinfarction HF. We found that changes in any individual current are relatively small, and alone could mislead as to consequences. However, differential changes in multiple currents integrate to shorten AP in the infarct border zone but prolong AP in the remote zone, increasing AP repolarization inhomogeneity. Our findings help explain why single channel-blocker therapy may fail, and highlight the need to understand the integrated changes of ionic currents in treating arrhythmias in HF.

PHYSIOLOGY

additional decrease of L-type Ca^{2+} current (I_{CaL}), decrease of inward rectifier K^+ current (I_{K1}), and arrhythmogenic sarcoplasmic reticulum (SR) Ca^{2+} release-induced delayed after-depolarizations (DADs). An unexpected finding is that the changes in any individual currents are relatively small, but differential changes in multiple currents integrate at the cell level to shorten AP duration (APD) in the border zone but prolong APD in the remote zone. Such inhomogeneous remodeling increases the difference in AP polarization between the border and the remote zones that may enhance the arrhythmogenic substrate. The integrated changes in ionic currents and spontaneous Ca^{2+} events increase the propensity for both triggered and reentrant arrhythmias.

The main strategy for antiarrhythmic drug development in recent decades has been to identify the culprit ion channels responsible for arrhythmias and develop specific ion channel blockers (or activators) to target individual channels. However, clinical trials of ion channel blockers have met unexpected failure, as summarized by Sanderson (8) in the Editorial on SWORD and CAST II trials: "In few specialties of medicine are new promising

drugs shown to be so much inferior to placebo and, even worse, to increase mortality." The present study sheds new light into this important problem by using an innovative approach to measure the complex electrophysiological changes in a large-animal model of chronic post-MI HF. Our findings provide in-depth mechanistic insights into why blocking a single ion channel may fail to suppress arrhythmias and highlights the need for developing more comprehensive strategies to correct multifaceted electrophysiological changes in ischemic HF.

Results

Structural Remodeling and Systolic Dysfunction in Ischemic HF. To provide a clinically relevant large-animal ischemic HF model, we subjected adult Yucatan minipig to microbead embolization of the first diagonal branch of the left anterior descending coronary artery (LAD), which caused transmural MI and a progressive reduction in the EF. At the time of study (5 mo post-MI) the HF pig hearts exhibited well-healed transmural scars (Fig. 1A), a 36% reduction in EF (Fig. 1B and Table S1), and dilated cardiomyopathy
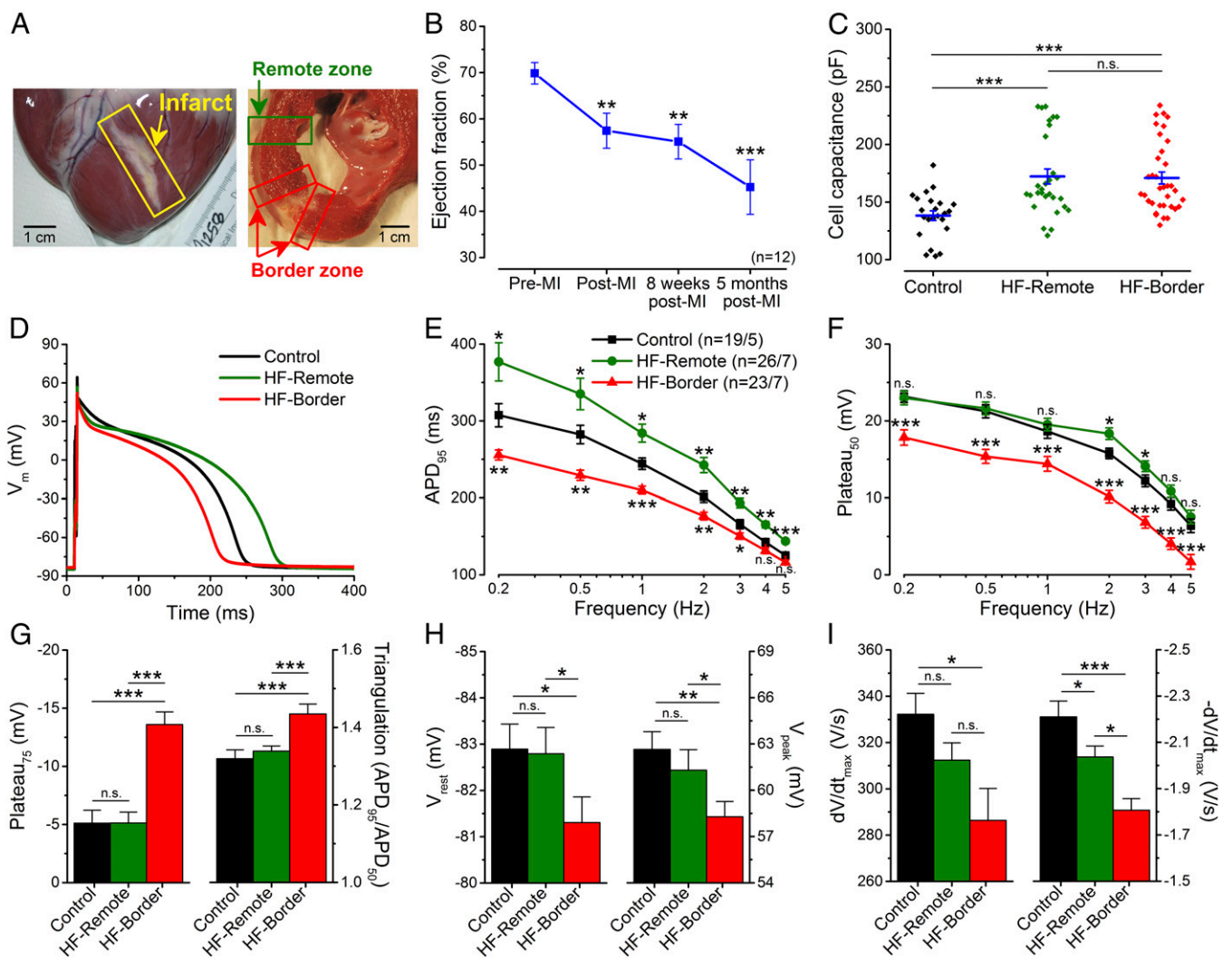
Fig. 1. Altered AP morphology in ischemic HF. (A) Photomicrograph of an infarcted heart showing the border zone and the remote zone. (B) LV EF significantly decreased 5 mo after MI induction (n = 12 animals). (C) Cell capacitance increased significantly in failing cardiomyocytes. (D) Representative APs recorded in control, HF-remote, and HF-border cells at 1-Hz pacing frequency (at 36 °C). (E) HF-remote cells have increased APD_{95} while HF-border cells have decreased APD_{95}. (F) Frequency-dependence of $Plateau_{50}$. (G) Significantly altered $Plateau_{75}$ and AP triangulation in HF-border cells. (H) V_{rest} is slightly more positive in HF-border cells, in line with decreased V_{peak}. (I) dV/dt_{max} is decreased only in the HF-border, while $-dV/dt_{max}$ is significantly decreased in both HF zones. Mean ± SEM, n = 19–26 cells/5–7 animals. ANOVA with Bonferroni posttest; n.s., not significant, *P < 0.05, **P < 0.01, ***P < 0.001.

(with 41% increase of end-diastolic volume and 116% increase of end-systolic volume) (Table S1). Post-MI pigs exhibited clinical signs of congestive HF, such as abdominal ascites fluid and pulmonary edema after 5 mo post-MI, but not within 8 wk post-MI, indicating the progression of the disease. Compared with healthy control pig ventricular myocytes, HF myocytes also showed significant hypertrophy (measured by electrical capacitance) (Fig. 1C), demonstrating structural remodeling at the cellular level.

Heterogenous Changes of AP Morphology in Ischemic HF. HF myocytes underwent distinct changes in AP morphology (Fig. 1D), demonstrating functional remodeling. Compared with control, myocytes from the infarct border zone (HF-border) showed shortened APD (measured at 95% repolarization, APD_{95}), whereas myocytes from the remote zone (HF-remote) showed prolonged APD_{95} (Fig. 1E). The above APD_{95} differences between cell groups remained significant over a range of pacing frequencies (0.2–5 Hz), while APD_{95} in each cell group progressively decreased with increasing pacing frequency (Fig. 1E). These data reveal heterogeneous remodeling of AP that gives rise to significant APD dispersion from infarct border to remote zones, creating an enhanced substrate for arrhythmias.

Moreover, plateau potentials ($Plateau_{50}$, $Plateau_{75}$) were decreased in the HF-border but remained unchanged in the HF-remote (Fig. 1F), which increased the AP triangulation factor in the HF-border (Fig. 1G). Resting membrane potential (V_{rest}) was slightly depolarized in the HF-border (Fig. 1H, Left), concomitant with a slight decrease of the AP peak voltage (V_{peak}) (Fig. 1H,

Right) and the maximal upstroke velocity (dV/dt) (Fig. 1I, Left). The maximal rate of phase 3 repolarization ($-dV/dt$) was decreased drastically in the HF-border, and moderately in the HF-remote (Fig. 1I, Right). These data indicate complex and differential changes in the underlying ionic currents that cause APD dispersion in HF.

Furthermore, the short-term variability (STV) of APD_{95} was also significantly increased in the HF-remote (Fig. S2 A and B), with a larger percentage of beats exhibiting more than 5- and 10-ms difference from beat to beat (Fig. S2 C and D). This increased temporal variability of APD_{95} provides an additional substrate for arrhythmias, as previously inferred in human chronic ischemic HF (9).

Triggered Activities and Spontaneous SR Ca^{2+} Leak in Ischemic HF. After-depolarizations are known to occur more frequently in HF (1). Under baseline steady-state pacing conditions, we did not observe early after-depolarizations (EAD). We also evaluated DADs immediately after myocyte pacing at 5 Hz for 3 min (Fig. 2A). We found significant increases of DADs and triggered APs (tAPs) in HF-border and HF-remote cells compared with control (Fig. 2 B and C), with HF-border cells exhibiting DADs with larger amplitudes and tAPs at higher frequency than that of HF-remote (Fig. 2C).

Next, we tested the mechanism of DADs in HF. These DADs were eliminated by inhibiting I_{NCX} (Fig. S4 A–D), consistent with DADs originating from the inward I_{NCX} induced by spontaneous SR Ca^{2+} releases (10). Furthermore, I_{K1} density was decreased in
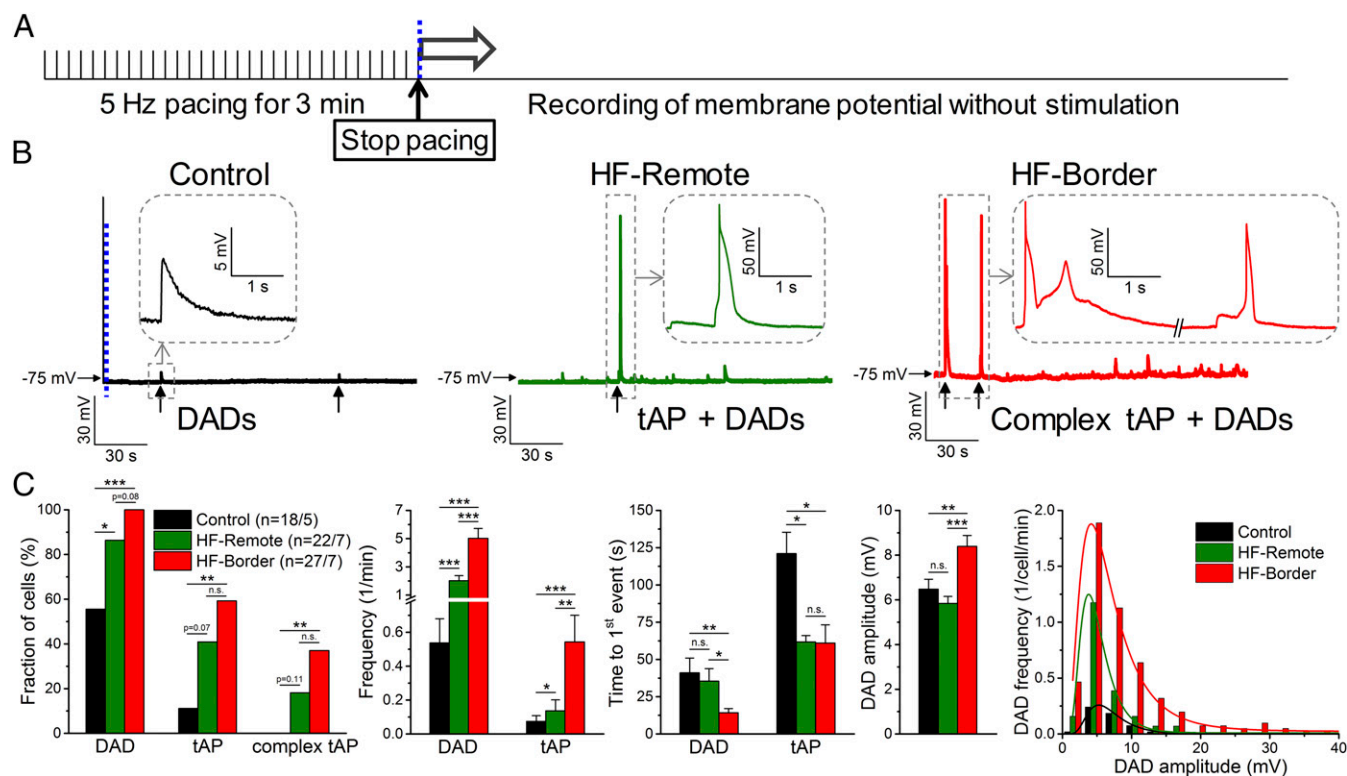
Fig. 2. Arrhythmogenic diastolic activities in ischemic HF. (A) DADs and tAPs were elicited following cessation of 3 min of burst pacing (5 Hz). (B) Representative records in control, HF-remote, and HF-border cells. Ten of 18 control cells showed a few DADs with small amplitude (enlarged in Inset). The last paced beat is shown before the blue dashed line, indicating the cessation of pacing for comparison in magnitude. Nineteen of 22 HF-remote cells showed DADs with a much higher frequency than in control, and among those cells 9 of 22 also showed tAPs (enlarged in Inset). All HF-border cells showed DADs and 16 of 27 cells also showed tAPs, often with an EAD superimposed on the tAP repolarization (complex tAP, enlarged in Inset). (C) Statistics of the arrhythmogenic diastolic events. DAD parameters were assessed only in those events where no tAP occurred subsequently. DAD amplitude data were fitted to a lognormal distribution curve ($R^2 = 0.99$ in both cases). Mean ± SEM, $n = 18$–27 cells/5–7 animals. Fisher's exact test and ANOVA with Bonferroni posttest; n.s., not significant, *$P < 0.05$, **$P < 0.01$, ***$P < 0.001$.

the HF-border (Fig. S3), which would allow any given inward I_{NCX} to cause greater membrane depolarization. Moreover, inhibition of Ca^{2+}–calmodulin-dependent protein kinase II (CaMKII) decreased DADs to the control level (Fig. S4 *F–H*), implying that pathological CaMKII activation causes SR Ca^{2+} leak, in agreement with prior HF findings in canine (11) and rabbit (12) models.

To directly examine the SR Ca^{2+} leak in our porcine HF model, we measured diastolic Ca^{2+} sparks, which were markedly increased in frequency and duration in HF-border myocytes (Fig. S5). Hence, the above data suggest that increased SR Ca^{2+} leak causes DADs and tAPs, especially in the HF-border, which may trigger arrhythmias in ischemic HF.

Intracellular Ca^{2+} Transient and Myocyte Contraction in Ischemic HF.
Given the intertwined nature of electrophysiology and Ca^{2+} signaling, we also measured the intracellular Ca^{2+} concentration ($[Ca^{2+}]_i$) and cell contraction during field-stimulated APs in ventricular myocytes (Fig. 3, at 22 °C; Fig. S6, at 36 °C). Notably, $[Ca^{2+}]_i$ transient amplitudes at 0.5 Hz pacing were comparable in both HF zones (Fig. 3B) and in control at room temperature, although the $[Ca^{2+}]_i$ decline rate (τ) was slower, and the diastolic $[Ca^{2+}]_i$ was slightly increased in HF (Fig. 3 *A* and *C*). In contrast, contraction was significantly decreased in both HF zones compared with control (Fig. 3B). Because Ca^{2+} handling processes are temperature-dependent, $[Ca^{2+}]_i$ transients were also compared in the HF-border vs. HF-remote at body temperature. Again, no significant difference was found between the two HF zones (Fig. S6), consistent with warming accelerating all Ca^{2+} transport systems, but without altering relative contributions appreciably (13). This result contrasts with a previous study in sheep showing markedly lower $[Ca^{2+}]_i$ transients and cell contractions in border vs. remote zones in 8-wk post-MI myocytes without HF (3). Our 5-mo post-MI porcine hearts may be remodeled during the HF progression in a way that limits differences between HF-border and HF-remote $[Ca^{2+}]_i$ transients. With little change in $[Ca^{2+}]_i$ transient, decreased contraction suggests that a decrease of the myofilament Ca^{2+} responsiveness (in both border and remote zones) might be responsible for reduced EF in this HF model. In the following studies, we focus further on the electrophysiological changes that contribute to arrhythmogenesis.

Remodeling of Inward Currents in Ischemic HF. To measure the ionic currents that shape the AP, we used ^{self}AP-clamp sequential dissection for several reasons. First, ^{self}AP-clamp uses each cell's own steady-state AP as command voltage during ionic current recording; this enables us to measure currents during that cell's physiological AP and with preserved $[Ca^{2+}]_i$ transients. Second, sequential dissection of ionic currents (as a specific blocker-sensitive current)

allows recording of multiple currents from the same cell (Fig. S1 and Table S2); enabling us to measure both inward and outward currents that shape the AP. Third, recording eight different ionic currents in each of a limited number of failing porcine hearts is a unique advantage of our ^{self}AP sequential dissection approach, much more efficient than conventional voltage-clamp studies of only one ionic current per myocyte. We will first examine the changes in each ionic current, and then investigate how these changes collectively reshape the AP and arrhythmogenic substrate in HF.

I_{NaL} (recorded as a GS-458967–sensitive current under ^{self}AP-clamp) showed a persistent inward current during AP plateau (Fig. 4A). I_{NaL} became larger as a driving force ($V_m−E_{Na}$) increased gradually during AP repolarization. In HF-remote cells, I_{NaL} was increased during the plateau and repolarization phases, causing an increased total Na^+ entry during the AP cycle. In HF-border cells, I_{NaL} also had increased plateau and peak values, but the integrated total Na^+ entry was not different from control because of shortened APD_{95} (Fig. 4).

I_{NCX} (measured with a new selective inhibitor, ORM-10962) was outward (Ca^{2+} influx) early in the AP and then turned inward during the $[Ca^{2+}]_i$ transient (Ca^{2+} efflux), peaking during rapid repolarization in control cells (Fig. 4A). However, in both HF-remote and HF-border cells, outward I_{NCX} was not observed but was inward throughout the AP (Fig. 4A). Inward I_{NCX} density increased during the midplateau in HF myocytes, despite exhibiting similar $[Ca^{2+}]_i$ transients as control (Fig. 3A), which drives inward I_{NCX}. This is consistent with an increased functional NCX in HF (10), especially for HF-remote, where midplateau V_m was not different from control (Fig. 1F). However, neither I_{NCX} (during phase 3) nor integrated total charge movement through inward I_{NCX} were significantly different among the three groups (Fig. 4).

I_{CaL} was measured as the nifedipine-sensitive current after blockade of other Ca^{2+}-dependent currents (details in *SI Materials and Methods* and Fig. S1). I_{CaL} reached its peak early in the AP plateau and gradually decreased during phases 2 and 3 of the AP (Fig. 4A). The peak I_{CaL} density, the midplateau value, and the total Ca^{2+} charge movement in HF-remote cells were similar to that of the control, but all of these measures were significantly decreased in the HF-border (Fig. 4B).

Remodeling of Outward Currents in Ischemic HF. I_{Kr} (measured as an E-4031–sensitive current) was small during the AP plateau, but increased during phase 3 repolarization (Fig. 5A). Peak I_{Kr} density was slightly decreased in both HF zones compared with control (Fig. 5 *A* and *B*). The slow delayed rectifier K^+ current (I_{Ks}, measured as an HMR-1556–sensitive current) rose gradually
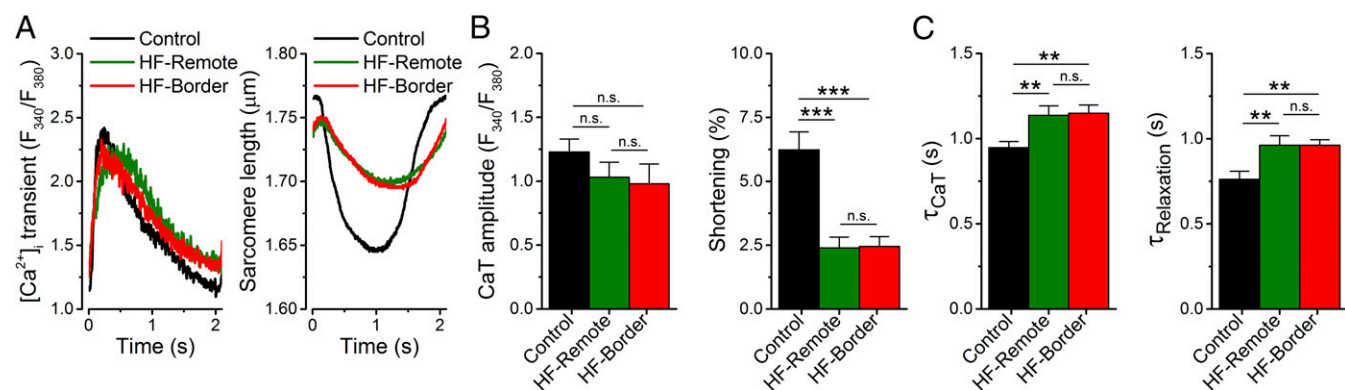
Fig. 3. Changes in $[Ca^{2+}]_i$ transient and contraction in ischemic HF. (A) Representative $[Ca^{2+}]_i$ transient and simultaneously recorded sarcomere shortening evoked by field stimulation at 0.5-Hz pacing frequency (at 22 °C). (B) No change was found in $[Ca^{2+}]_i$ transient amplitude; however, sarcomere shortening significantly decreased in both HF zones. (C) The time constants (τ) of $[Ca^{2+}]_i$ decline and relaxation were significantly increased in both HF zones. Mean ± SEM, n = 16–23 cells/5–7 animals. ANOVA with Bonferroni posttest; n.s., not significant, **P < 0.01, ***P < 0.001.

Hegyi et al.
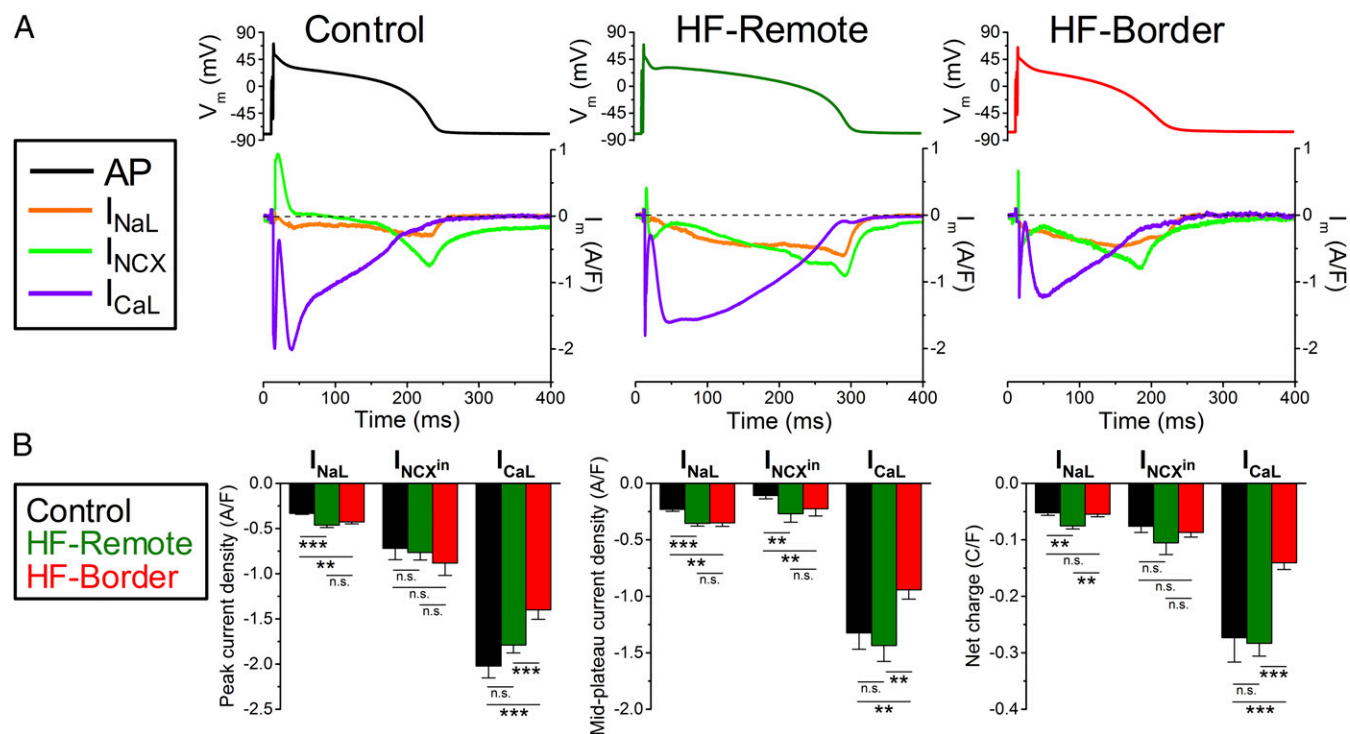
Fig. 4. Major inward currents during ventricular AP using ^self^AP-clamp technique. (*A*) Representative current traces measured under the cell's own AP at 1-Hz steady-state pacing in the control, HF-remote, and HF-border. Panels above show the APs used as voltage commands. GS-458967, ORM-10962, and nifedipine were used to record late Na⁺ current (I_{NaL}), Na⁺/Ca²⁺ exchanger current (I_{NCX}), and L-type Ca²⁺ current (I_{CaL}), respectively. (*B*) Peak and midplateau current densities as well as net charges carried by the corresponding ion channels. Mean ± SEM, $n = 6–16$ cells/4–6 animals. ANOVA with Bonferroni posttest; n.s., not significant, **$P < 0.01$, ***$P < 0.001$.

during the plateau and declined during repolarization, but I_{Ks} density was much smaller than I_{Kr} (Fig. 5*A*). Peak I_{Ks} density and the total charge moved were unaltered in either the HF zone vs. control (Fig. 5*B*). I_{K1} (measured as a Ba²⁺-sensitive current) rose rapidly at the end of phase 3 repolarization and had a sustained component during diastole (Fig. 5*A*). Peak I_{K1} density was unchanged in the HF-remote, but was significantly decreased in the HF-border (Fig. 5*B*). The midplateau I_{K1}, but not the diastolic I_{K1} was increased in the HF-border, consistent with altered I_{K1} rectification in the HF-border (Fig. 5*B*). Total charge carried by I_{K1} was decreased in the HF-border but not in the HF-remote vs. control (Fig. 5*B*).

Remodeling of Ca²⁺-Activated Currents in Ischemic HF. As a significant advantage, the ^self^AP-clamp technique allows us to record the dynamic profile of Ca²⁺-activated currents under the cell's steady-state AP with preserved [Ca²⁺]$_i$ transient in physiological milieu. $I_{Cl(Ca)}$ (measured as a 9-anthracenecarboxylic acid-sensitive current) was a large outward current during early repolarization, but declined during the plateau, turning inward during rapid repolarization (as V_m passed the expected Cl⁻ reversal potential) (Fig. 5*A*). Both peak outward and inward $I_{Cl(Ca)}$ and integrals were higher in the HF-remote and HF-border vs. control (Fig. 5*C*). Moreover, inward diastolic $I_{Cl(Ca)}$ significantly increased in both HF zones vs. control (Fig. 5*C*).

A small $I_{K(Ca)}$ (measured as an apamin-sensitive current) was detected during the AP (Fig. 5*A*), comparable in size to I_{Ks} in control. However, $I_{K(Ca)}$ increased significantly in both HF zones, often with a hump coinciding with the larger peak of $I_{Cl(Ca)}$ (Fig. 5).

Relative Contributions of Different Ionic Currents in Reshaping APs in Ischemic HF. V_m is determined instantaneously by counterbalancing

inward and outward currents, such that the AP is shaped by integrating all ionic currents. Figs. 4 and 5 show the magnitude and time course of each ionic current during the AP. The contribution of a particular current on the AP at any time point is determined by its relative strength compared with all other currents (Fig. 6 and Fig. S1). To understand the relative contribution of each current to AP shape, we calculated total depolarization drive (DD) as the sum of all inward currents and the total repolarization drive (RD) as the sum of all outward currents (net currents in Fig. 6). We also express each current as percent of DD or RD at each point in time (Fig. 6, ionic fingerprints).

Among the depolarizing currents, in healthy controls (Fig. 6, *Left*) I_{CaL} is the largest inward current during the AP plateau phase, much larger than I_{NaL} and I_{NCX}. Fast Na⁺ current (I_{Na}) during AP upstroke would saturate the amplifier and was not recorded (>50 times larger than peak I_{CaL}). However, during late repolarization (phase 3), I_{NaL} and I_{NCX} gain more influence, and $I_{Cl(Ca)}$ also becomes inward, contributing to DD. At terminal AP repolarization, I_{NCX} becomes the dominant inward current, and remains the dominant inward current in phase 4. Compared with control, HF-remote myocytes (Fig. 6, *Center*) show decreased I_{CaL} but increased I_{NaL} and I_{NCX}. In the HF-border (Fig. 6, *Right*), the changes in these inward currents follow the same trend but are more pronounced, with the relative contribution of $I_{NaL} + I_{NCX}$ doubled at the AP midplateau time point.

Among the repolarizing currents, in healthy controls (Fig. 6, *Left*, *Lower*) phase 1 early repolarization of the AP is mainly caused by the outward $I_{Cl(Ca)}$ current, with minor contribution from the reverse-mode I_{NCX}. In porcine myocytes, transient outward K⁺ current (I_{to}) was not detectable. Hence, in this species, $I_{Cl(Ca)}$ rather than I_{to} is the main early repolarizing current. At midplateau of the AP, the relative contribution of several repolarizing currents [$I_{Cl(Ca)}$, $I_{K(Ca)}$, I_{Kr}, I_{Ks}, I_{K1}] is about equal (∼20%
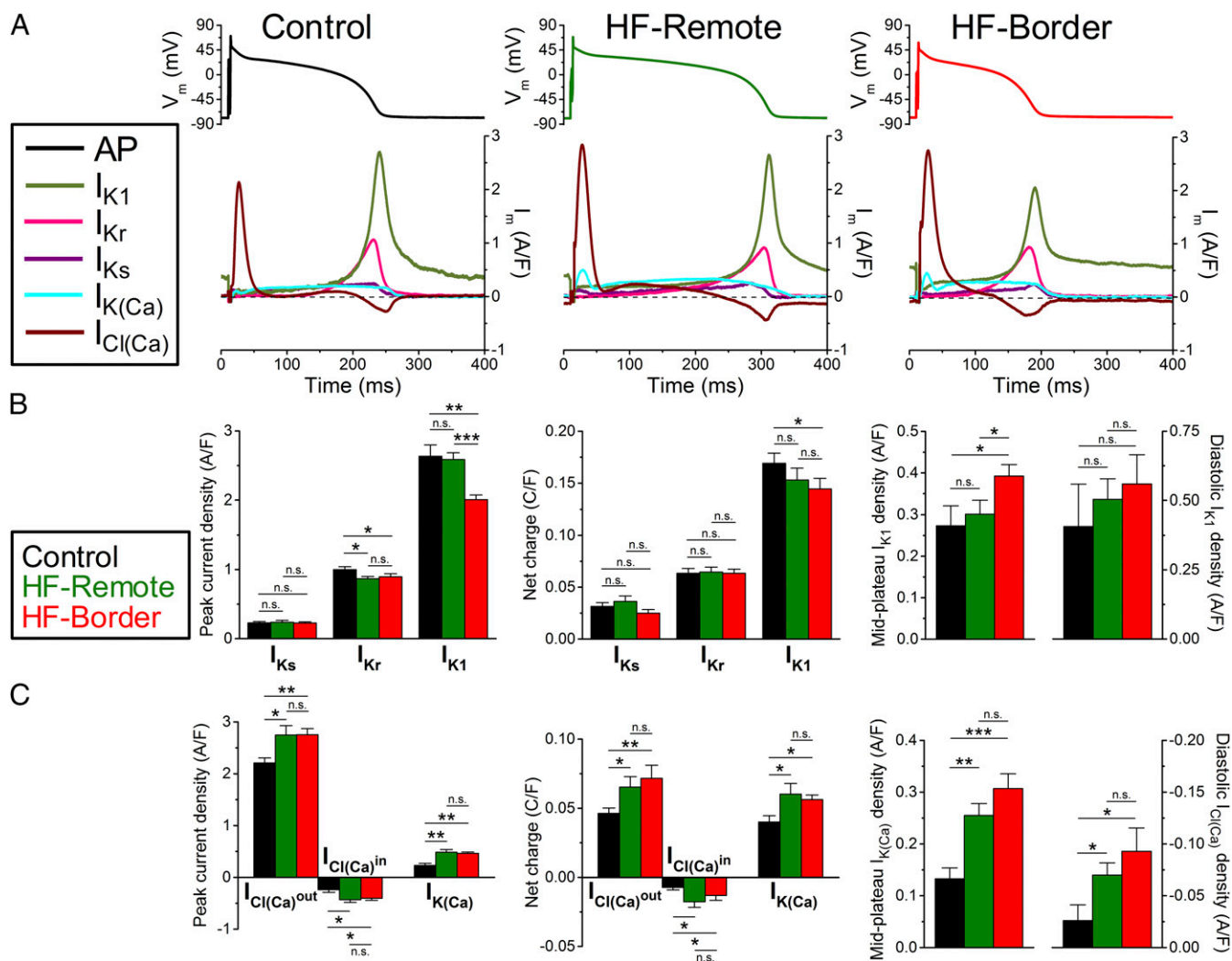
Fig. 5. Major outward currents during ventricular AP using ^{self}AP-clamp technique. (*A*) Representative current traces measured under the cell own AP at 1-Hz steady-state pacing in the control, HF-remote, and HF-border. Panels above show the APs used as voltage commands. E-4031, HMR-1556, and Ba^{2+} were used to record rapid and slow delayed rectifier K$^+$ currents (I_{Kr} and I_{Ks}), and inward rectifier K$^+$ current (I_{K1}), respectively. Apamin and 9-anthracenecarboxylic acid were used to record Ca^{2+}-activated K$^+$ and Cl$^-$ currents [$I_{K(Ca)}$ and $I_{Cl(Ca)}$], respectively. (*B*) Peak current densities and net charges carried by I_{Kr}, I_{Ks}, and I_{K1}, as well as midplateau and diastolic density of I_{K1}. (*C*) Peak current densities and net charges carried by $I_{K(Ca)}$, inward and outward $I_{Cl(Ca)}$, as well as midplateau and diastolic density of $I_{Cl(Ca)}$. Mean ± SEM, n = 6–16 cells/4–6 animals. ANOVA with Bonferroni posttest; n.s., not significant, *$P < 0.05$, **$P < 0.01$, ***$P < 0.001$.

of RD). Compared with the control, in HF-Remote (Fig. 6, *Center*, *Lower*) the outward I_{NCX} during phase 1 is diminished; $I_{K(Ca)}$ is increased during the plateau phase and I_{K1} is decreased. In the HF-border (Fig. 6, *Right*, *Lower*), changes of these outward currents follow the same trend, but the magnitude of changes are more pronounced. Important to the coupling between Ca^{2+} signaling and electrical systems, the contribution of Ca^{2+}-activated currents [$I_{K(Ca)}$, $I_{Cl(Ca)}$] to the total repolarizing drive are significantly increased [$I_{K(Ca)} + I_{Cl(Ca)}$ ~50% of RD] at midplateau in both the HF-border and HF-remote cells. The ionic fingerprints in Fig. 6 succinctly convey comprehensive information on the relative power of different ionic currents to shape the AP and the relative contribution of each current to electrophysiological remodeling in ischemic HF.

Discussion

Here we study a large-animal model of chronic ischemic HF to understand increased susceptibility to cardiac arrhythmias. Prior large-animal studies considered earlier stages post-MI (2–7 d) or

relatively early after MI healing (8 wk) (2, 5). Our study on a 5-mo post-MI porcine model with chronic HF is unique in determining the long-term remodeling of ionic currents in chronic ischemic HF. We found that the APD is shortened in the infarct border zone but lengthened in the remote zone. Our APD data agree generally with prior findings of shortened APD in the border zone of healed infarct in cat (14), but prolonged remote-zone ventricular APD from rabbit (10), canine (15), and human hearts (16). Importantly, we systematically studied differential changes between border and remote zones, revealing heterogeneous remodeling in post-MI HF, increasing the inhomogeneity of ventricular AP repolarization. Furthermore, we provide mechanistic insights of the underlying ionic bases for the AP profile changes.

In studying depolarizing currents, I_{CaL} was previously found decreased or unchanged as a result of two opposing effects: decreased expression and increased phosphorylation of the channel protein in the ventricular myocytes isolated from human HF (16). We found that I_{CaL} density and integral during the AP
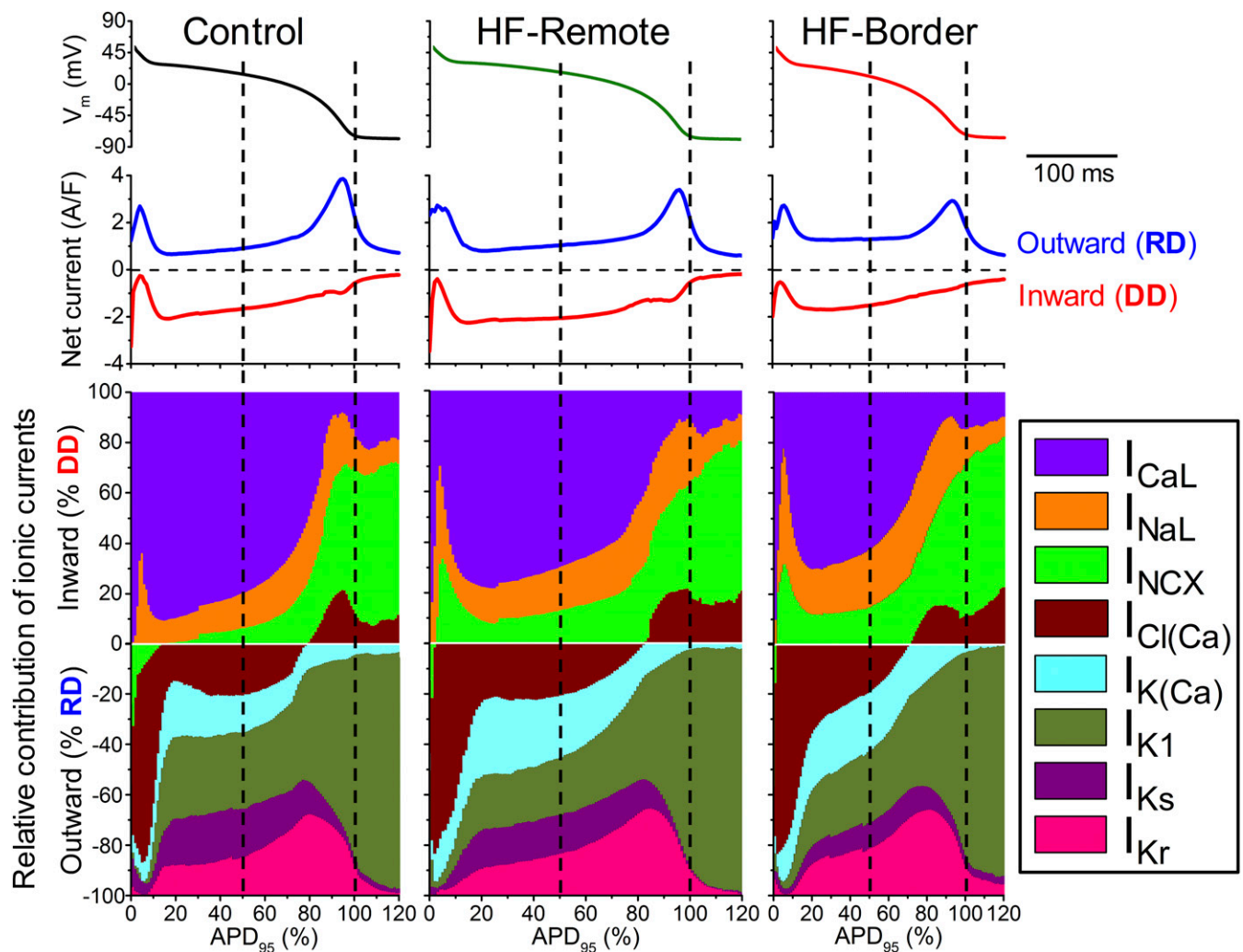
Fig. 6. Dynamical relations of ionic currents during the AP. The contribution of each inward and outward current was normalized to the momentary total outward (RD) or inward (DD) membrane current calculated based on the measured eight ionic current densities. Ionic currents measured in each cell were also normalized to the corresponding APD_{95}. Vertical dashed lines correspond to $Plateau_{50}$ and APD_{95}.

was significantly decreased only in HF-border zone but not in HF-remote zone ventricular myocytes. I_{NaL} has been recorded as a tiny Na^+ current under voltage-clamp, and was slightly increased in HF (15). Here we show that the I_{NaL} under ^{self}AP-clamp is a sustained inward current throughout the AP plateau, shaping the APD and increasing the Na^+ entry during AP. I_{NaL} is markedly increased in HF.

Previously, I_{NCX} was found to be up-regulated in HF, which causes larger inward I_{NCX} during spontaneous SR Ca^{2+} release, thereby increasing DADs and triggered arrhythmia susceptibility (10, 17). Here we used a selective NCX inhibitor ORM-10962 to record the dynamic I_{NCX} during the AP. In control myocytes, I_{NCX} was briefly outward early in the AP, but then predominantly inward throughout the remainder of the AP peaking during rapid repolarization. This is similar to prior indirect I_{NCX} measurements during the AP in rabbit and human ventricular myocytes (18). In post-MI HF, there was no early outward I_{NCX}, and inward I_{NCX} was a sustained current during the plateau (Fig. 4). This finding differs from the above rabbit and human HF results, where I_{NCX} was outward through much of the AP plateau. The difference may be attributable to better maintained $[Ca^{2+}]_i$ transients in our failing porcine hearts (Fig. 3) and possibly less rise in $[Na^+]_i$, both of which would favor more inward I_{NCX}. The higher inward I_{NCX} observed here during the plateau (with similar $[Ca^{2+}]_i$ transients)

is consistent with functional up-regulation of NCX in our porcine model. Hence, the overall I_{NCX} dynamics during AP promotes earlier Ca^{2+} extrusion in HF than in control.

In studying repolarizing currents, reduced repolarization reserve and altered repolarization currents are hallmarks of HF (19, 20). Previous studies reported that delayed rectifier K^+ currents were decreased or unchanged in HF (1). We found no change in basal I_{Ks}, which is relatively small in the absence of β-adrenergic stimulation, and only a slight decrease in I_{Kr} during AP in the both HF zones. I_{K1} is reportedly decreased in human and rabbit HF (10, 19). We recorded I_{K1} dynamics during AP and found that peak I_{K1} density is significantly decreased in the HF-border, but unaltered in the HF-remote. Interestingly, mid-plateau I_{K1} is increased in the HF-border, consistent with altered I_{K1} rectification, which is attributed to intracellular Mg^{2+} and polyamines that could be altered in HF (21, 22). I_{K1} represents the dominant outward current in AP repolarization (phase 3) and during diastole (where it stabilizes resting V_m).

Na/K-ATPase pump current (I_{NKA}, not measured here) contributes a smaller diastolic outward current (vs. I_{K1}). I_{NKA} is expected to be larger during the AP plateau, and similar in amplitude (~0.3 A/F) (23) to the four currents measured here [$I_{Cl(Ca)}$, $I_{K(Ca)}$, I_{Kr}, and I_{Ks}] that dominate during the AP plateau (Figs. 5 and 6). Moreover, increases in $[Na^+]_i$, which are known

to occur in HF, ischemia, and rapid heart rates, would promote larger outward I_{NKA} and outward I_{NCX}. Because the overall conductance is low during the AP plateau, relatively small changes in these Na^+- and Ca^{2+}-dependent currents can significantly impact repolarization and APD (23).

The Ca^{2+}-activated K^+ and Cl^- currents have rarely been considered in shaping ventricular APs. Here we recorded $I_{K(Ca)}$ and $I_{Cl(Ca)}$ under ^{self}AP-clamp with $[Ca^{2+}]_i$ transient and demonstrated that these two currents are significant in the control and HF porcine myocytes, and both currents are further increased in HF. Previous studies also reported up-regulation of $I_{K(Ca)}$ in human cardiomyocytes independent of $[Ca^{2+}]_i$ changes (24). $I_{Cl(Ca)}$ was increased HF in rabbit, but not in human (25). Here we show that $I_{Cl(Ca)}$ is increased in porcine HF. Furthermore, our data reveal that the increased outward $I_{Cl(Ca)}$ and $I_{K(Ca)}$ counteract the increased inward currents (I_{NaL}, I_{NCX}) during the AP plateau in HF.

The ^{self}AP-clamp with sequential current analysis is powerful in showing how multiple ionic currents behave during the physiological AP in a single myocyte. Nonetheless, the absolute precision for each individual current may be limited by the cumulative addition of relatively channel-selective agents and time course of experiments. To this end, the low diastolic levels of I_{Kr}, I_{Ks}, and I_{CaL} indicated in Fig. 6 are likely close to zero, but are exaggerated graphically because total DD and RD are quite small during diastole (and that is pressing the precision limits of the method). Moreover, the main likely diastolic inward currents that balance outward $I_{K1} + I_{NKA}$ at the stable resting potential are probably I_{NCX}, Na^+ leak, and Ca^{2+} leak. In addition, there is evidence for a TTX-sensitive diastolic leak that is increased in HF (26), and so may be mediated by Na^+ channels.

HF involves not only remodeling of ionic currents and APs but also diastolic arrhythmogenic events. DADs were frequently observed in HF, providing the arrhythmogenic trigger (10, 25). We also found significantly increased DADs and triggered APs. The DADs were mediated by I_{NCX} [not by $I_{Cl(Ca)}$], similar to previous findings in rabbit and human HF (10, 25). Moreover, we found that the late Na^+ current, elevated diastolic $[Ca^{2+}]_i$, and CaMKII-dependent SR Ca^{2+} leak all contribute to significantly increasing the frequency of DADs and tAPs, particularly in the infarct border zone. Hence, in porcine chronic ischemic HF, DADs and tAPs are significantly increased and contribute as triggers for initiating arrhythmias, in conjunction with significantly different APD between HF-remote and HF-border cells that may enhance the substrate for reentrant arrhythmias.

Limitations

One limitation of using a porcine model for human translational relevance is our observed lack of I_{to} in pig myocytes, which contributes to transmural AP differences in the human heart. Myocardial infarction and remodeling may also affect the transmural regions differently, which could influence the AP dispersion. However, because I_{to} is significantly reduced in HF (1), the lack of I_{to} in pig may not be a major limitation for differential repolarization remodeling in infarct border vs. remote zones in HF. The ultimate test would come from studying human cardiac myocytes, which is limited by the availability of adult human HF hearts. Applying the AP-clamp sequential dissection method could aid future human myocyte study. Moreover, a systematic study of Ca^{2+} handling in different ventricular regions and at various pacing rates would further inform the arrhythmogenic mechanisms in ischemic HF. We also did not induce arrhythmias in vivo or in isolated heart optical mapping studies because of the cost of the chronic porcine model, limited number of animals available, and other parallel uses of these pigs. Inducibility of unidirectional block and reentry requires steep APD differences over relatively short distances. Here, the border and remote zones from which myocytes were isolated

were roughly 1–1.5 cm apart, but we cannot provide further spatial detail, and hence cannot comment on APD gradient steepness in vivo. Finally, in relating single-cell electrophysiology to arrhythmogenesis in the heart, one must also consider other important factors, including the electrical coupling between cells, fibrosis and mechanical load effects, as well as neurohormonal changes that modify cardiac excitation–contraction coupling in HF.

Conclusion and Perspectives

Our data reveal that chronic ischemic HF involves remodeling of a multitude of ion channels and exchangers heterogeneously in the infarct border and remote zones. Even though no individual current shows dramatic changes, the integration of small changes from multiple ionic currents significantly remodel the AP profile. Differential changes in multiple currents integrate at the cell level to shorten APD in the border zone but prolong APD in the remote zone, giving rise to pronounced dispersion of APD at the tissue level. Such emerging APD dispersions with both long-QT and short-QT substrates create imbalanced electrophysiology landscape to promote arrhythmias in post-MI ischemic HF. Our findings demonstrate that in-depth mechanistic understanding requires comprehensive studies of many ionic currents and suggest a framework for precision therapeutics. Indeed, the complex changes of ion channels in HF support the hypothesis that drugs influencing multiple ion channels (e.g., amiodarone, ranolazine) may provide more effective treatment if the integrated effects can rebalance the electrophysiology landscape. Moreover, drugs reducing pathological SR Ca^{2+} leak (e.g., CaMKII inhibitors) and drugs targeting defective neurohormonal regulations that influence complex changes in multiple ion channels, may also have advantages in suppressing arrhythmias. Given that the strategy of targeting single-ion channels has met failures, the comprehensive analysis that we have done here provide integrated approaches and rich data to inform future development of new strategies for treating arrhythmias in ischemic heart failure.

Materials and Methods

Details are provided in *SI Materials and Methods*.

Animals. Four- to 6-mo-old adult Yucatan minipigs were subjected to microbead embolization of the first diagonal branch of the LAD, which caused transmural MI and progressive reduction in EF over 5 mo (Table S1), at which time left ventricular (LV) myocytes were isolated. The porcine model of chronic MI used is this study was developed to provide a clinically relevant large-animal ischemic cardiomyopathy model, as previously described (6). Cardiomyocytes from the remote or border zone of the infarct were obtained by enzymatic digestion using cannulation and perfusion of the left coronary vasculature. As control, cardiomyocytes were isolated from the same region of the heart of healthy age-matched sham control minipigs. All animal handling and laboratory procedures followed US National Institutes of Health guidelines and were approved by the Institutional Animal Care and Use Committee of the University of California, Davis.

Electrophysiology. Recordings were performed in isolated ventricular cardiomyocytes using whole-cell patch-clamp with physiological solutions at 36 °C (for ionic composition, see *SI Materials and Methods*). APs were evoked in current-clamp experiments where cells were stimulated with short suprathreshold depolarizing pulses at 0.2- to 5-Hz pacing frequencies delivered via the patch pipette. Ionic currents during the AP were measured using ^{self}AP-clamp with physiological solutions (at 1-Hz pacing), preserved $[Ca^{2+}]_i$ cycling, and sequential block of specific ionic currents (Fig. S1 and *SI Material and Methods*) using selective ion channel inhibitors (Table S2), as previously described (7, 27).

$[Ca^{2+}]_i$ Transient and Myocyte Contraction. Parallel $[Ca^{2+}]_i$ transients and contractions were assessed by Fura-2 fluorescence ratio (F_{340}/F_{380}) and sarcomere length measurements in field-stimulated myocytes (at 22 °C and 36 °C, as indicated, and 0.5-Hz pacing) using an IonOptix system, as previously described (28).

Confocal Imaging of Ca^{2+} Signals. Diastolic Ca^{2+} sparks were detected by Fluo-4 fluorescence in intact myocytes (at 22 °C) using an Olympus FluoView FV1000 confocal microscope, as previously described (28).

Echocardiography. Averaged data from three consecutive cardiac cycles were obtained in 2D and M-mode assessments using the standard LV outflow tract view. Animals were in dorsal recumbency during imaging with a S5-1 linear probe (Philips Healthcare) under anesthesia (during MI induction) or deep sedation (during follow-up at 8 wk and 5-mo post-MI).

Statistical Analysis. Averaged data are presented as mean $\pm$ SEM. The number of cells in each experimental group was reported as n = number of cells/number of animals, and the cells in each group came from three to seven individual animals. Statistical significance of differences was evaluated using ANOVA to compare multiple groups and Bonferroni posttest was used for pairwise comparisons for continuous variables. Categorical outcomes were evaluated using Fisher's exact test. A value of $P < 0.05$ was considered significant.

1. Tomaselli GF, Marbán E (1999) Electrophysiological remodeling in hypertrophy and heart failure. *Cardiovasc Res* 42:270–283.
2. Dun W, Baba S, Yagi T, Boyden PA (2004) Dynamic remodeling of K+ and Ca2+ currents in cells that survived in the epicardial border zone of canine healed infarcted heart. *Am J Physiol Heart Circ Physiol* 287:H1046–H1054.
3. Kim YK, et al. (2002) Altered excitation-contraction coupling in myocytes from remodeled myocardium after chronic myocardial infarction. *J Mol Cell Cardiol* 34:63–73.
4. Shimkunas R, et al. (2013) Left ventricular myocardial contractility is depressed in the borderzone after posterolateral myocardial infarction. *Ann Thorac Surg* 95:1619–1625.
5. Yuan F, et al. (1999) Characteristics of I(K) and its response to quinidine in experimental healed myocardial infarction. *J Cardiovasc Electrophysiol* 10:844–854.
6. Hanes DW, et al. (2015) Embolization of the first diagonal branch of the left anterior descending coronary artery as a porcine model of chronic trans-mural myocardial infarction. *J Transl Med* 13:187.
7. Banyasz T, Horvath B, Jian Z, Izu LT, Chen-Izu Y (2011) Sequential dissection of multiple ionic currents in single cardiac myocytes under action potential-clamp. *J Mol Cell Cardiol* 50:578–581.
8. Sanderson J (1996) The SWORD of Damocles. *Lancet* 348:2–3.
9. Piccirillo G, et al. (2007) QT variability strongly predicts sudden cardiac death in asymptomatic subjects with mild or moderate left ventricular systolic dysfunction: A prospective study. *Eur Heart J* 28:1344–1350.
10. Pogwizd SM, Schlotthauer K, Li L, Yuan W, Bers DM (2001) Arrhythmogenesis and contractile dysfunction in heart failure: Roles of sodium-calcium exchange, inward rectifier potassium current, and residual beta-adrenergic responsiveness. *Circ Res* 88:1159–1167.
11. Johnson DM, et al. (2013) Diastolic spontaneous calcium release from the sarcoplasmic reticulum increases beat-to-beat variability of repolarization in canine ventricular myocytes after β-adrenergic stimulation. *Circ Res* 112:246–256.
12. Ai X, Curran JW, Shannon TR, Bers DM, Pogwizd SM (2005) Ca2+/calmodulin-dependent protein kinase modulates cardiac ryanodine receptor phosphorylation and sarcoplasmic reticulum Ca2+ leak in heart failure. *Circ Res* 97:1314–1322.
13. Puglisi JL, Bassani RA, Bassani JW, Amin JN, Bers DM (1996) Temperature and relative contributions of Ca transport systems in cardiac myocyte relaxation. *Am J Physiol* 270:H1772–H1778.
14. Wong SS, et al. (1982) Dissimilarities in the electrophysiological abnormalities of lateral border and central infarct zone cells after healing of myocardial infarction in cats. *Circ Res* 51:486–493.
15. Valdivia CR, et al. (2005) Increased late sodium current in myocytes from a canine heart failure model and from failing human heart. *J Mol Cell Cardiol* 38:475–483.
16. Chen X, et al. (2002) L-type Ca2+ channel density and regulation are altered in failing human ventricular myocytes and recover after support with mechanical assist devices. *Circ Res* 91:517–524.
17. Hasenfuss G, et al. (1999) Relationship between Na+-Ca2+-exchanger protein levels and diastolic function of failing human myocardium. *Circulation* 99:641–648.
18. Weber CR, Piacentino V, 3rd, Ginsburg KS, Houser SR, Bers DM (2002) Na(+)-Ca(2+) exchange current and submembrane [Ca(2+)] during the cardiac action potential. *Circ Res* 90:182–189.
19. Beuckelmann DJ, Näbauer M, Erdmann E (1993) Alterations of K+ currents in isolated human ventricular myocytes from patients with terminal heart failure. *Circ Res* 73:379–385.
20. Hegyi B, et al. (2018) Altered repolarization reserve in failing rabbit ventricular myocytes: Calcium and β-adrenergic effects on delayed- and inward-rectifier potassium currents. *Circ Arrhythm Electrophysiol* 11:e005852.
21. Zaza A, Rocchetti M, Brioschi A, Cantadori A, Ferroni A (1998) Dynamic Ca2+-induced inward rectification of K+ current during the ventricular action potential. *Circ Res* 82:947–956.
22. Meana C, et al. (2016) Correlation between endogenous polyamines in human cardiac tissues and clinical parameters in patients with heart failure. *J Cell Mol Med* 20:302–312.
23. Grandi E, Pasqualini FS, Bers DM (2010) A novel computational model of the human ventricular action potential and Ca transient. *J Mol Cell Cardiol* 48:112–121.
24. Yu CC, et al. (2015) Small conductance calcium-activated potassium current is important in transmural repolarization of failing human ventricles. *Circ Arrhythm Electrophysiol* 8:667–676.
25. Verkerk AO, et al. (2001) Ionic mechanism of delayed afterdepolarizations in ventricular cells isolated from human end-stage failing hearts. *Circulation* 104:2728–2733.
26. Despa S, Islam MA, Weber CR, Pogwizd SM, Bers DM (2002) Intracellular Na(+) concentration is elevated in heart failure but Na/K pump function is unchanged. *Circulation* 105:2543–2548.
27. Chen-Izu Y, Izu LT, Hegyi B, Bányász T (2017) Recording of ionic currents under physiological conditions: Action potential-clamp and 'Onion-Peeling' techniques. *Modern Tools of Biophysics*, ed Jue T (Springer, New York), pp 31–48.
28. Jian Z, et al. (2014) Mechanochemotransduction during cardiomyocyte contraction is mediated by localized nitric oxide signaling. *Sci Signal* 7:ra27.

PHYSIOLOGY